Boundary-Layer Meteorol (2014) 152:1–18
DOI 10.1007/s10546-014-9914-6

ARTICLE

A Velocity–Dissipation Lagrangian Stochastic Model for Turbulent Dispersion in Atmospheric Boundary-Layer and Canopy Flows

Tomer Duman · Gabriel G. Katul · Mario B. Siqueira · Massimo Cassiani

Received: 29 August 2013 / Accepted: 3 February 2014 / Published online: 2 March 2014

Abstract An extended Lagrangian stochastic dispersion model that includes time variations of the turbulent kinetic energy dissipation rate is proposed. The instantaneous dissipation rate is described by a log-normal distribution to account for rare and intense bursts of dissipation occurring over short durations. This behaviour of the instantaneous dissipation rate is consistent with field measurements inside a pine forest and with published dissipation rate measurements in the atmospheric surface layer. The extended model is also shown to satisfy the well-mixed condition even for the highly inhomogeneous case of canopy flow. Application of this model to atmospheric boundary-layer and canopy flows reveals two types of motion that cannot be predicted by conventional dispersion models: a strong sweeping motion of particles towards the ground, and strong intermittent ejections of particles from the surface or canopy layer, which allows these particles to escape low-velocity regions to a high-velocity zone in the free air above. This ejective phenomenon increases the probability of marked fluid particles to reach far regions, creating a heavy tail in the mean concentration far from the scalar source.

Keywords Canopy · Dispersion · Dissipation · Lagrangian stochastic model

T. Duman (✉)
Nicholas School of the Environment, Duke University, Durham, NC, USA
e-mail: tomer.duman@duke.edu

G. G. Katul
Department of Civil and Environmental Engineering, Nicholas School of the Environment, Duke University, Durham, NC, USA

M. B. Siqueira
Department of Mechanical Engineering, Universidade de Brasília, Brasília, Brazil

M. Cassiani
The Norwegian Institute for Air Research (NILU), Oslo, Norway

1 Introduction

High Reynolds-number turbulence is characterized by pronounced intermittency in its small-scale structure, where the velocity gradients and the instantaneous turbulent kinetic energy (TKE) dissipation rate ϵ^* exhibit large fluctuations in time (Chen 1971). Experiments have repeatedly shown that the Eulerian probability density function (PDF) of the squared velocity gradient is characterized by stretched exponential tails, indicating rare and intense bursts in ϵ^* over relatively short periods of time (Frisch 1996). During these bursts, the flow exhibits unusually large local acceleration, evidenced by recent Lagrangian particle measurements (Porta et al. 2001). For atmospheric boundary-layer (ABL) flows, intermittency in ϵ^* can play a significant role, where the ratio between ϵ^* and its time-averaged value ($= \epsilon$) can reach as high as 50 (Pope 2000). This ratio may be larger inside canopies, where intermittency effects are likely to be much higher (Finnigan 2000).

This intermittent behaviour in ϵ^* can have a significant impact on how Lagrangian stochastic (LS) particle trajectory approaches model dispersion, which frames the compass of this work. LS models often used in atmospheric dispersion studies (e.g. Thomson 1987; Wilson and Sawford 1996) typically do not account for intermittency in ϵ^*. They estimate a local Lagrangian time scale as a function of a local ϵ. Although such models have been used extensively for calculating concentrations and flux footprint of gases, aerosols, particles, pollen, and seeds in both atmospheric and canopy flows (Flesch and Wilson 1992; Baldocchi 1997; Kurbanmuradov and Sabelfeld 2000; Rannik et al. 2000; Kljun et al. 2002; Nathan et al. 2002; Cassiani et al. 2005a,b; Poggi et al. 2006; Vesala et al. 2008; Hsieh and Katul 2009), they are based on the assumption of a layer-wise constant but vertically inhomogeneous Lagrangian time scale formed by the mean TKE and the mean dissipation rate ϵ.

Pope and Chen (1990) suggested using an extended LS model that includes not only the instantaneous velocity, but also the instantaneous dissipation (ϵ^*) along a particle trajectory, thus introducing time fluctuations for the dissipation rate for the first time. In this model, ϵ^* is sampled from a log-normal PDF, by solving an additional stochastic differential equation for $\chi \equiv \ln(\epsilon^*/\epsilon)$. This model relies on the hypothesis that in high Reynolds-number flows, ϵ^* is log-normally distributed (Kolmogorov 1962; Obukhov 1962), which was later shown to be valid in homogeneous isotropic turbulence from experiments (Monin and Yanglom 1975) and from direct numerical simulation (DNS) calculations (Yeung and Pope 1989).

This model, hereafter referred to as the log-normal model, was previously applied to several flow types, including turbulent wall-bounded flows (Pope 1991; Minier and Pozorski 1999), swirling flows (Anand et al. 1993) and mixing layers (Pope 1991). In these works, the log-normal model was employed for retracing the so-called super-statistics of turbulence, showing good performance in reproducing higher-order moments of the velocity (skewness and kurtosis). This log-normal model is extended here to include scalar dispersion, focusing specifically on atmospheric turbulence. The motivation is to explore the effects of high intermittency in ϵ^* on LS dispersion models for ABL and canopy flows. Establishing a correct dispersion model for these types of flows is becoming necessary for a large number of applications including inverse models that are aimed at inferring scalar sources and sinks from mean concentration profile measurements (Raupach 1989; Flesch et al. 1995; Leuning et al. 2000; Nemitz et al. 2000; Siqueira et al. 2000; Kljun et al. 2002; Siqueira et al. 2002, 2003; Simon et al. 2005; Juang et al. 2006; Tiwary et al. 2007).

To begin quantifying the effects of $\epsilon^* \neq \epsilon$ on dispersion, LS trajectory calculations of marked fluid particles are conducted with and without the addition of an equation describing the time variations of χ. As a case study, a thermally stratified ABL flow is first considered, where the inhomogeneity in ϵ is monotonic with height z from the ground. Another case study

explores a neutrally stratified canopy flow, where the inhomogeneity in ϵ is not monotonic with z. The resulting dispersion patterns with the addition of an equation for χ (the log-normal model) are then compared with the standard LS model (Thomson 1987), which includes the effects of a vertical variation of ϵ on dispersion without consideration of the variability in ϵ^* over time.

The paper commences with a brief review of the theoretical description of the extended stochastic model, which is formulated for a two-dimensional fully-developed inhomogeneous turbulent flow (Sect. 2). This formulation is achieved by coupling Thomson's (1987) standard LS model with the log-normal model for χ as proposed by Pope and Chen (1990). Although it is established that the instantaneous dissipation rate in the ABL exhibits a log-normal PDF (Chen 1971), there is no previous information about its behaviour inside dense canopies. Hence, in Sect. 3, this characteristic is further investigated using simultaneous multi-level velocity measurements collected inside a pine forest described elsewhere (Katul and Albertson 1998). These experiments empirically suggest that ϵ^*/ϵ is sufficiently large to warrant the addition of an equation for χ. The coupled velocity-χ formulation is then assessed via the so-called well-mixed condition (Thomson 1987), which is a necessary prerequisite for any LS model. In Sects. 4 and 5, the log-normal model for χ is employed to conduct trajectory simulations in atmospheric flow systems. The conventional case of a stationary and planar-homogeneous high Reynolds-number ABL flow in the absence of subsidence is first considered with velocity statistics described by Monin–Obukhov similarity theory. Marked fluid particles are released from a continuous elevated source and steady-state concentration fields are computed across different levels of thermal stratification for both the log-normal model and the standard LS model. In Sect. 5 the log-normal model is applied next to a canopy flow configuration, where the flow statistics are computed from a detailed second-order closure model. The advantage of this second-order closure model is that it solves an actual transport equation for ϵ (Siqueira et al. 2012). The comparison between the conventional LS model and the log-normal model focuses on dispersion patterns, peak concentration values and locations, and decay rates with distance from the release location.

2 The Velocity–Dissipation Lagrangian Stochastic Model

The formulation of the LS model is based on the generalized Langevin equation, which is used to compute trajectories of marked fluid particles, representing a scalar parcel (Thomson 1987; Rodean 1996),

$$\mathrm{d}u_{pi} = a_i \mathrm{d}t + b_{ij} \mathrm{d}W_j, \tag{1}$$

$$\mathrm{d}x_{pi} = \left(u_{pi} + \overline{u}_i\right) \mathrm{d}t. \tag{2}$$

It is assumed that the position of the particle x_{pi} and its Lagrangian turbulent velocity fluctuation u_{pi} along its trajectory both evolve as a Markov process. Here, $\overline{u}_i$ is the Eulerian mean velocity of the fluid along the particles trajectory, and dW is an incremental Wiener process with a zero mean and a variance of $\mathrm{d}t$. The sub-indexes i and $j = 1, 2, 3$ with repeated indexes imply summation. The coordinates $x_1 = x, x_2 = y, x_3 = z$ are aligned so that x_1 is along the longitudinal or mean wind direction, x_2 is the lateral direction, and x_3 is the vertical direction. The velocity components $u_1 = u, u_2 = v, u_3 = w$ are the velocity components aligned along x, y, z, respectively. Since only two-dimensional cases are considered, i and j each take on values of 1 and 3.

To satisfy both Kolmogorov's hypothesis of local isotropy in the Lagrangian frame of reference and the well-mixed condition (Thomson 1987), the diffusion ($=b_{ij}$) and drift ($=a_i$) terms in Eq. 1 take the following form for the fully-developed two-dimensional case according to Thomson's (1987) simplest solution (for notational convenience a_1, a_3, b_{11}, and b_{33} are replaced with a_u, a_w, b_u, and b_w respectively),

$$a_u = -\frac{b_u^2}{A}\left(\sigma_w^2 u_\mathrm{p} - \overline{u'w'}w_\mathrm{p}\right) + \frac{1}{2}\frac{\partial \overline{u'w'}}{\partial z} + \frac{1}{A}\left[\sigma_w^2 \frac{\partial \sigma_u^2}{\partial z} u_\mathrm{p} w_\mathrm{p} - \overline{u'w'}\frac{\partial \sigma_u^2}{\partial z} w_\mathrm{p}^2 - \overline{u'w'}\frac{\partial \overline{u'w'}}{\partial z} u_\mathrm{p} w_\mathrm{p} + \sigma_u^2 \frac{\partial \overline{u'w'}}{\partial z} w_\mathrm{p}^2\right], \quad (3)$$

$$a_w = -\frac{b_w^2}{A}\left(\sigma_u^2 w_\mathrm{p} - \overline{u'w'}u_\mathrm{p}\right) + \frac{1}{2}\frac{\partial \sigma_w^2}{\partial z} + \frac{1}{A}\left[\sigma_w^2 \frac{\partial \overline{u'w'}}{\partial z} u_\mathrm{p} w_\mathrm{p} - \overline{u'w'}\frac{\partial \overline{u'w'}}{\partial z} w_\mathrm{p}^2 - \overline{u'w'}\frac{\partial \sigma_w^2}{\partial z} u_\mathrm{p} w_\mathrm{p} + \sigma_u^2 \frac{\partial \sigma_w^2}{\partial z} w_\mathrm{p}^2\right], \quad (4)$$

$$b_u = b_w = \sqrt{C_0 \epsilon^*}, \quad (5)$$

$$A = 2\left(\sigma_w^2 \sigma_w^2 - \overline{u'w'}^2\right), \quad (6)$$

where σ_u, σ_w are the Eulerian velocity standard deviations in the horizontal and vertical directions (x and z), and $\overline{u'w'}$ is the Reynolds stress. C_0 is the Lagrangian Kolmogorov constant for the Lagrangian structure function taken to be 3.125 based on a matching of the Lagrangian time scale to similarity theory (Li and Taylor 2005). Traditionally, the diffusion term b (Eq. 5) is calculated using ϵ. To include fluctuations in the dissipation rate, ϵ is replaced with ϵ^*. Following Pope and Chen (1990), the quantity $\chi \equiv \ln(\epsilon^*/\epsilon)$ is defined to be normally distributed when ϵ^* is log-normally distributed. To include the memory effects of χ, it is treated as a Markov process whose dynamics can be described by an additional Langevin equation given as,

$$\mathrm{d}\chi = -\left(\chi - \langle\chi\rangle\right)\frac{\mathrm{d}t}{T_\chi} + \sqrt{\frac{2\sigma^2}{T_\chi}}\mathrm{d}W, \quad (7)$$

where σ is the standard deviation (SD) of χ, $\langle\chi\rangle$ is its ensemble mean that must be set to $-0.5\sigma^2$ (Pope and Chen 1990), and T_χ is the Lagrangian integral time scale of χ. Equation 7 is valid only for Gaussian homogeneous turbulence. Pope (1991) extended the log-normal model to include inhomogeneous flows. While Eq. 7 introduces only two new parameters (σ and T_χ), the stochastic model for inhomogeneous flows is much more complex, and includes additional parameters that are difficult to estimate a priori. Also, this extension is justified by the need to correct for possible non-log-normality in the dissipation rate distribution. Instantaneous dissipation rate measurements for both ABL and canopy flows appear to behave approximately log-normal as shown in Sect. 3. Hence, as a logical starting point, Eq. 7 is employed despite the vertical inhomogeneity in the flow. As shown later, this simplified model is able to generate a realistic time evolution of instantaneous dissipation rates.

To use Eq. 7, the parameters σ and T_χ must be determined. T_χ is taken to be $T_\chi^{-1} = C_\chi \omega$, where ω is the mean turbulent frequency that is defined as the ratio between the mean dissipation rate and the mean TKE $\omega \equiv \epsilon/k$. Originally, Pope and Chen (1990) set the value of $C_\chi = 1.6$, based on moderate Reynolds-number DNS runs for homogeneous isotropic turbulence (Yeung and Pope 1989), to yield a ratio of $T_\mathrm{L}/T_\chi = 0.9$ (T_L is the Lagrangian integral time scale of the turbulent velocity fluctuation). This value may be incompatible

with ABL and canopy flows, due to the fact that they are not homogeneous and isotropic and the Reynolds number and turbulent intensity are much higher than those reported for these DNS runs. The sensitivity of the log-normal model to the values of C_χ is further examined in Sect. 4; the value of σ defines the width of χ's distribution and is discussed in details in Sect. 3.

3 The Probability Distribution of the Dissipation Rate in Canopy Flows

To explore the PDF of the dissipation rate in canopy flows, multi-level field measurements from a uniform pine forest are used (Katul and Albertson 1998). From the time series of the measured velocity at five levels, four inside and one above the canopy, the value of χ can be estimated by the approximation $\chi \approx \ln\left[(\partial u/\partial t)^2 \,/\, \overline{(\partial u/\partial t)^2}\right]$. Figure 1 shows that the mean SD of the approximated χ for the pine forest is approximately constant, with a value of 2.5, for all levels within the canopy. Above the canopy, a somewhat higher value is observed with a wider spread across different runs (each run representing a 30-min sampling duration). The calculated values from the pine forest far exceed the value of $\sigma = 1$, chosen originally by Pope and Chen (1990) according to their DNS runs. This higher σ represents an increased intermittent behaviour with more frequent events experiencing higher dissipation rate values than ϵ.

The PDF of χ from the field experiment, shown in Fig. 2a, resembles a Gaussian distribution. However some skewness may be observed, where the large negative excursions in χ have lower probability of occurrences and large positive excursions in χ have lower magnitudes when compared to a normal distribution. A probability plot test (Fig. 2b) reveals the PDF deviations from a Gaussian distribution, which is displayed in this type of plot as a straight line with a slope set to the inverse of the SD. The same skewed behaviour was previously observed in ABL measurements by Chen (1971), Antonia (1973), and Freytag (1978). Chen's (1971) results, which are shown also in Fig. 2a for reference, produce almost the same PDF as the canopy flow results reported here, with similar values for both the mean and the SD of χ. Freytag (1978) relates this behaviour to the use of the approximated dissipation rate formulation, and shows from ABL measurements that using the exact definition of the dissipation of TKE ($\epsilon = 0.5\nu(\partial u_i/\partial x_j + u_j/\partial x_i)^2$) produces a Gaussian PDF

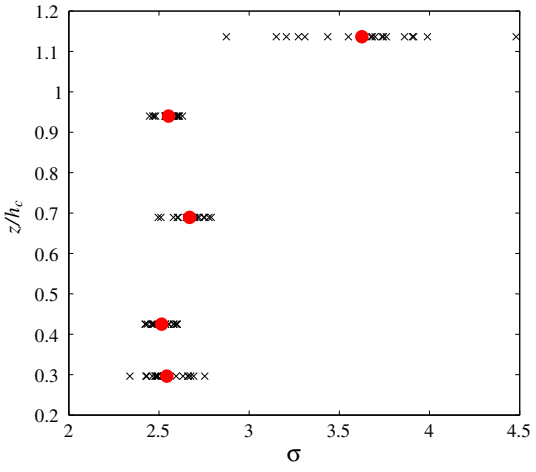

Fig. 1 The profiles of the dissipation SD χ, calculated from pine forest experiments (the x's indicate 30-min 10-Hz measurement runs, and the *dots* are the mean values)

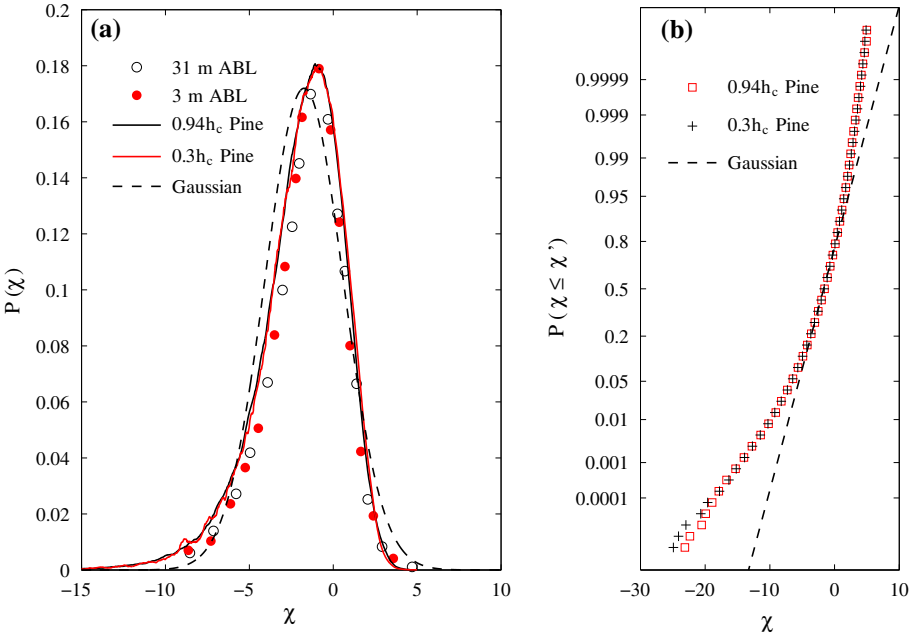

Fig. 2 **a** PDF of χ, calculated from the pine forest experiments. Compared with ABL measurements (Chen 1971) and with a fitted Gaussian distribution. **b** A probability plot test of the pine forest experiment, with the corresponding Gaussian distribution

for χ. Chen (1971) attributes this skewness and also the fact that the measurement shows $\langle\chi\rangle \neq -0.5\sigma^2$ to an inconsistency in the original definition of Kolmogorov and Obukhov of the local dissipation rate, which should be averaged over a sphere of radius r instead of a point measurement. Such a correction reconstructs a Gaussian PDF with lower values for σ, but still higher than unity ($\sigma \approx 1.7$), and a mean of $-0.5\sigma^2$.

It can be surmised that the dissipation rate is log-normally distributed even for canopy flows, and that the large calculated values of σ justify incorporating the time variability of the dissipation rate in the LS model. To test the sensitivity of the log-normal model to the value of σ, two scenarios are examined: one with $\sigma = 1$ as suggested originally by Pope and Chen (1990), and another using the upper limit from the in-canopy measurements (i.e. $\sigma = 2.5$).

4 Application to the Atmospheric Boundary Layer

Satisfying the well-mixed condition (Thomson 1987) is an important prerequisite for correct dispersion simulations. The model proposed here includes PDFs of dissipation and velocity that are independent, and its formulation satisfies the well-mixed condition, as shown in Appendix 1. This has been verified thoroughly by conducting a numerical test, showing that an initially released well-mixed concentration of particles in a highly inhomogeneous canopy flow remained well-mixed with an error of less than 2 % for all combinations of σ and C_χ values. The details of the well-mixed test and its results are also presented in Appendix 1. After checking that the model satisties the well-mixed condition as expected, it is now employed in trajectory simulations for a fully-developed ABL.

4.1 ABL Simulation Details

Neutral, stable and unstable stability conditions are now considered with flow statistics determined from Monin–Obukhov similarity theory (MOST). The details of the Eulerian velocity statistics profiles for all stability conditions are provided in Appendix 2. For all the simulations, the friction velocity and aerodynamic roughness length were chosen to be $u_* = 0.4\,\mathrm{m\,s^{-1}}$ and $z_0 = 1.7$ mm, respectively.

The particle trajectory simulations included a continuous elevated source positioned at a height $z_s = 2$ m above the ground. All simulations lasted for 1.5 h during which 10^6 particles were released from the source. The particle locations were saved each 10 s and a steady state was determined as the time for which the number of particles remained constant in a window frame of $(x, z) = (200{,}000 \times 200)\,\mathrm{m}^2$. The timestep for the trajectory simulations was calculated dynamically as $dt = 0.02T_\mathrm{L}$ to satisfy the necessary condition that $\mathrm{d}t \ll T_\mathrm{L}$ (for details about the calculation of T_L see Appendix 2). Using smaller timesteps revealed negligible changes in the concentration results. For each timestep, the turbulent velocity fluctuations u_p and w_p were calculated using Eqs. 1 and 3–6, and the particle locations were determined from Eq. 2. The instantaneous dissipation was also calculated for each t by solving Eq. 7 for χ and obtaining $\epsilon^* = \epsilon\,\exp(\chi)$, which was then used for the calculation of the stochastic diffusion term b. With the addition of the log-normal model, a second limitation on the timestep is necessary to ensure that $\mathrm{d}t \ll T_\chi$. Furthermore, the timestep was limited to prevent large jumps in the vertical direction, so the chocice of $\mathrm{d}t$ was $\mathrm{d}t = \min(0.02T_\mathrm{L},\ 0.02T_\chi,\ z_\mathrm{max}/w(t - \mathrm{d}t))$, where z_max was set to 1 m.

The ground and the boundary-layer top (set at 1 km for neutral and unstable conditions, and 300 m for stable conditions) were taken to be perfect reflectors so as to conserve the total mass in the domain at all times. A particle that reached either the top of the boundary layer or the ground was perfectly reflected in the vertical direction with respect to the boundary, and the sign of its velocity fluctuations u_p and w_p was reversed. In practice, the ground was taken at a height of 50 mm to prevent unrealistic high values of ϵ, which becomes unbounded as $T_\mathrm{L} \to 0$ near the ground.

For ABL flows, the drift terms a_u and a_w (Eqs. 3, 4) reduce to a simple form. In the neutral and the stable cases, all the Reynolds stress terms are constant (σ_u, σ_w, and $\overline{u'w'}$), so Eqs. 3 and 4 are reduced to

$$a_u = -\frac{b_u^2}{A}\left(\sigma_w^2 u_\mathrm{p} - \overline{u'w'}w_\mathrm{p}\right), \tag{8}$$

and

$$a_w = -\frac{b_w^2}{A}\left(\sigma_u^2 w_\mathrm{p} - \overline{u'w'}u_\mathrm{p}\right), \tag{9}$$

respectively. However, the unstable conditions introduce vertical variability in the fluctuating velocity SD (i.e. σ_u, and σ_w), while the terms related to $\partial\overline{u'w'}/\partial z$ remain zero.

The simulations were performed with the standard LS model and the proposed log-normal model. Two values of $\sigma = 1$ and 2.5 were examined, as mentioned before, and the sensitivity to C_χ was further tested. Since C_χ is a measure of the relation between T_L and T_χ, we choose to check the originally suggested value of $C_\chi = 1.6$, as well as approximately doubling its value to 3 and reversing the relation by setting $C_\chi = 0.5$. At the end of the simulations, the mean concentration maps of particles were calculated based on the steady-state particle locations.

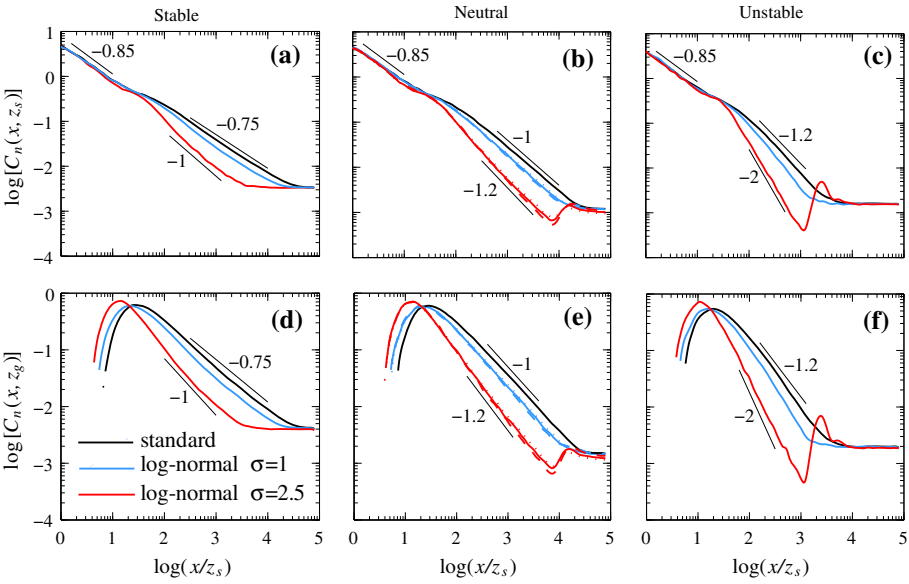

Fig. 3 Horizontal variation of normalized concentration $C_{\mathrm{n}} = \frac{C}{SI/u_r z_{\mathrm{s}}}$ as a function of distance from the source x for ABL flows. SI stands for source intensity and u_r is the wind velocity at source height. **a–c** present the horizontal variation at the source height (z_{s}) for stable, neutral and unstable conditions respectively. **d–f** are the same but at ground level (z_{g}). The *solid lines* in all sub-figures represent simulations with $C_\chi = 1.6$. For the neutral case (**b**, **e**), simulations of $C_\chi = 0.5$ and 3 are also shown by the *dashed lines* and the *dotted lines* respectively

4.2 Results

Figure 3 shows how the mean concentration C changes with increased downwind distance x from the source location. These C variations with x are presented at two heights: the source release height z_{s} (Fig. 3a–c), and ground level z_{g} (Fig. 3d–f). The downwind concentration variations with x at the source height reveal three distinct regions: a near-field and a far-field that exhibit approximate power laws with distinct exponents (i.e. $C(x, z_{\mathrm{s}}) \sim x^{\alpha}$), and a very far-field where the concentration attains a near constant value (i.e. $\mathrm{d}C(x, z_{\mathrm{s}})/\mathrm{d}x \approx 0$).

In Lagrangian fluid mechanics, the behaviour of near-field and far-field concentration variations with x have been recognized and defined analytically for turbulent diffusion when turbulent statistics are Gaussian and spatially homogeneous (Taylor 1921). These two fields are related to the ratio of the travel time t of an ensemble of passive particles since their release to the Lagrangian integral time scale T_{L}. In the near-field $t \ll T_{\mathrm{L}}$, the dispersion or spread is dominated by persistence of initial particle velocities through the drift term a, and the particle cloud size grows nearly linearly with t. In the far-field $t \gg T_{\mathrm{L}}$, the dispersion is dominated by the diffusion term (e.g. b), and the spread of the particle cloud is slower and grows as $t^{0.5}$. For inhomogeneous flows, the relation between travel time or distance and the particle cloud spread becomes more complicated, and a numerical analysis must be used to distinguish between the near-field and far-field behaviours.

In the results presented here (Fig. 3), the near-field appears concentrated in a short distance of $x \approx 20 z_{\mathrm{s}}$ downwind from the source. For $C(x, z_{\mathrm{s}})$ (Fig. 3a–c), this region is characterized by a rapid decay in $C(x, z_{\mathrm{s}})$ with increasing x. The exponent $\alpha = -0.85$ describing this decay appears insensitive to atmospheric stability or the addition of ϵ^*. As noted earlier,

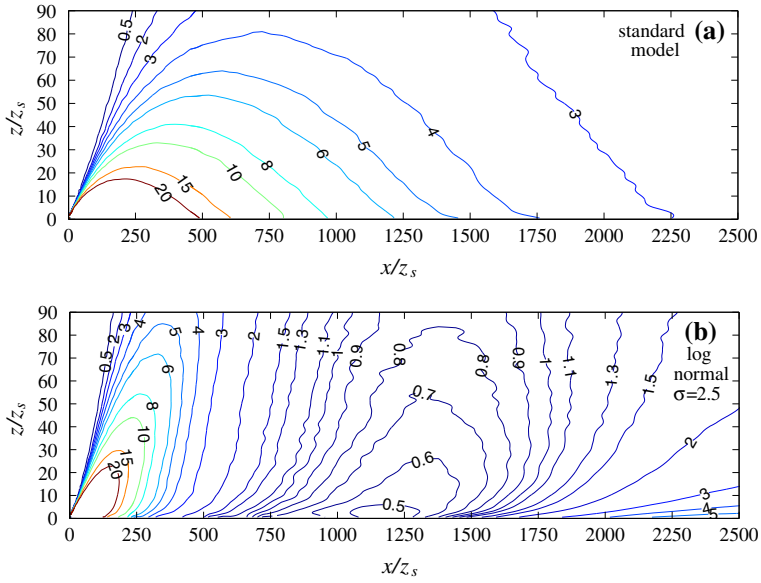

Fig. 4 Contour plots of the steady-state mean normalized concentration fields $C_n(x,z) = \frac{C(x,z)}{SI/u_r z_s}$ for unstable ABL flow. The figure presents values multiplied by 1,000 for convenience. The results are for **a** standard model, and **b** log-normal model conducted with $\sigma = 2.5$ and $C_\chi = 1.6$

this insensitivity can be attributed to the persistence of the initial velocity conditions of the particles near the release at z_s for all stability conditions. Moreover, the inclusion of ϵ^* is not likely to affect the near-field $C(x, z_s)$ variation with x since such addition mostly affects the diffusion term b of the Langevin equations that does not dominate the spread in the near-field.

For the mean concentration distribution with x at ground level (Fig. 3d–f), $C(x, z_g)$ rapidly increases with x in the near-field, until a peak value is reached. Here, the log-normal model shows a rapid increase in the mean concentration with x characterized by a peak concentration location closer to the source. The addition of ϵ^* generates a strong sweeping motion of particles from the source towards the ground, which occurs during bursts of high excursions in ϵ^*. Increasing the value of σ amplifies this effect, since these events become more frequent for $\sigma = 2.5$.

In the far-field, the decrease of $C(x, z_s)$ with x is much slower than its decrease in the near-field, similar to what occurs in homogeneous flows. In this region the normalized concentration drops by less than 0.1 over a distance of more than $1{,}000 z_s$. The decay exponent α in this region is the same for both the ground-level and the source-height concentrations. The addition of ϵ^* primarily increases the decay rate of $C(x, z_s)$ and $C(x, z_g)$ with x in this region. Hence, the very far-field steady-state concentration approaches a near constant value located closer to the source when compared to the standard LS model. Increasing σ increases the decay rate, and transitorily reduces the concentration below the final 'well-mixed' concentration state (for neutral and unstable conditions). The effect of the log-normal model on this region is expected, since it explicitly changes the stochastic diffusion term ($=b$) that dominates the far-field behaviour. Another type of particle motion that explains this difference in decay rate has been identified to be generated by the log-normal model. This motion is linked to strong intermittent ejections of particles from the surface layer to a higher velocity zone in the upper regions of the ABL coinciding with the mixed layer. This phenomenon is better shown in the mean concentration contour plot for unstable conditions (Fig. 4). In

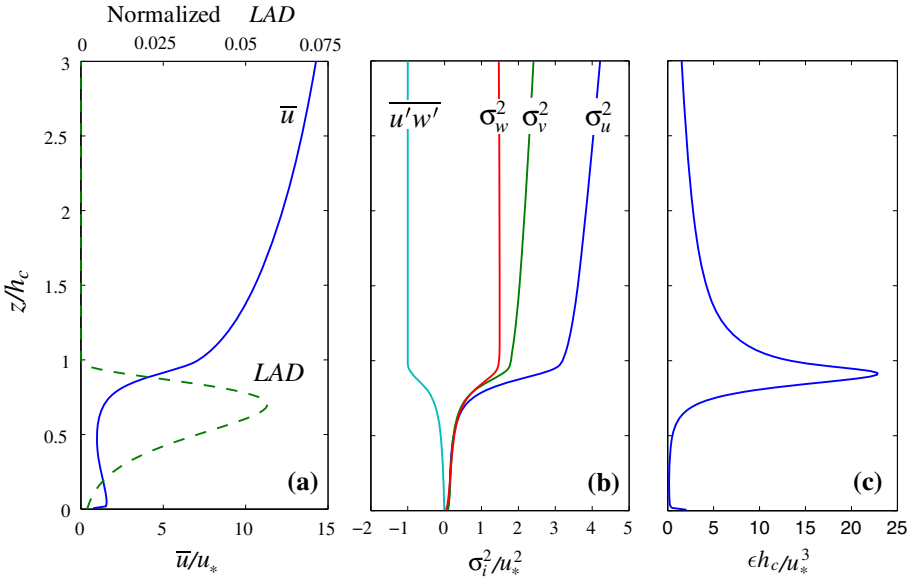

Fig. 5 The Eulerian flow statistics used for the canopy flow case study as computed by the second-order closure model

the log-normal model, the concentration rises to high values in the mixed-layer much closer to the source, compared with the standard model. Further from the source, the log-normal model generates a region of low concentrations near the ground. The ejected particles are finally mixed (due to reflecting boundary conditions), which induces further mixing so that the mean concentration decays with x in the mixed layer and increases near the ground.

The results show minor sensitivity to the value of C_χ for all the simulations that were conducted, as demonstrated for the neutral conditions in Fig. 3. This robustness to C_χ variations makes the log-normal model attractive, since it now requires one parameter, σ, that describes the entire behaviour of the instantaneous dissipation PDF.

5 Application to Canopy Flow

The log-normal formulation is now used to model dispersion for a canopy-flow configuration. For this type of flow, all vertical gradients in velocity statistics affect the drift and diffusion terms. Moreover, unlike the ABL case study earlier, ϵ does not monotonically decrease with increasing z. For dense canopies, it was shown that ϵ peaks around the canopy top (Fig. 5c); hence, an enhanced effect of the log-normal model may be expected in the upper parts of the canopy (Raupach and Thom 1981; Wilson 1988; Poggi et al. 2004).

The canopy-flow statistics were generated by solving a second-order one-dimensional closure model, which includes a transport equation for ϵ. This model, described elsewhere (Siqueira et al. 2012), was previously tested for dense canopies. The flow was solved for a friction velocity $u_* = 0.4\,\mathrm{m\,s^{-1}}$ defined at the canopy top, a foliage drag coefficient $C_\mathrm{d} = 0.1$ and a leaf area index $LAI = 3$, which was distributed unevenly with height as shown by the leaf area density (*LAD*) in Fig. 5a. The flow was solved to five times the canopy height (h_c), and a neutral ABL logarithmic profile was matched above this solution from $5h_\mathrm{c}$ to the top

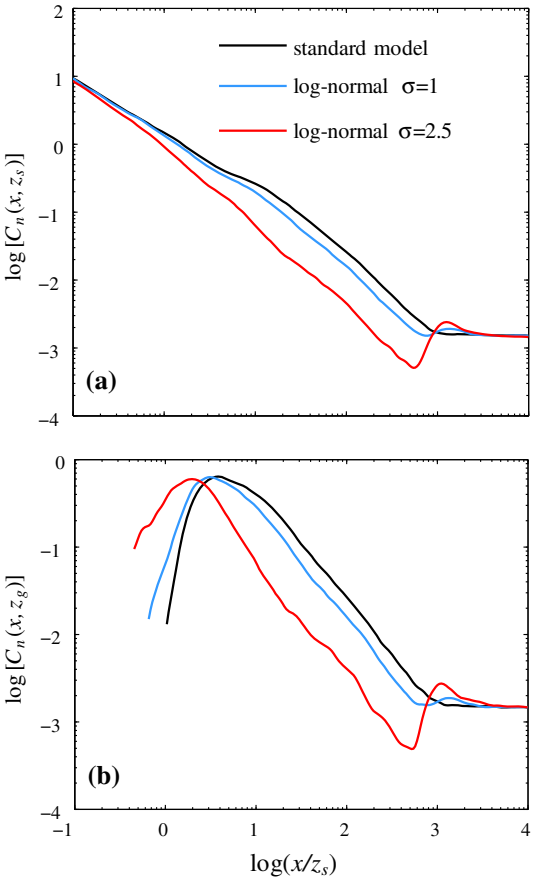

Fig. 6 The variation of the normalized concentration C_n as a function of distance x from the source for a canopy flow ($C_\chi = 1.6$): **a** at source height, and **b** at ground level

of the ABL (1 km). The flow statistics from the solution of the second-order closure model are presented in Fig. 5, and serve as an input to the LS models.

The source height was chosen to be at $0.8h_c$ of the canopy height, the layer where scalar source strength is expected to be largest for biologically active scalars such as water vapour or CO_2. The reason is that light interception, which drives stomatal opening, and high foliage concentration are roughly co-located in this vicinity (Siqueira et al. 2002; Juang et al. 2008). All other simulations details are identical to those for the ABL flow (Sect. 4).

Horizontal concentration variations (Fig. 6) show again three regions. The addition of the log-normal model affects the decay already in the near-field at the source height (Fig. 6a). The combination of low mean velocity and high dissipation value at the source height enhances the two types of particle motion discussed above: the sweeping motion towards the ground and the ejections of particles from inside the canopy to above. The sweeping motion creates again an increase in the concentration values near the ground, and shifts the concentration peak location closer to the source (Fig. 6b). Particles ejected above the canopy have a smaller chance to re-enter the canopy due to the rapid change in the gradients of the flow statistics near the canopy top. This effect is further amplified in the log-normal model by creating short events of high ϵ^* during which more ejections occur. In the far-field, the spatial decay rate of the mean concentration is similar to the standard and the log-normal models, and is also not affected by increasing σ from 1 to 2.5. In this region, the concentration within the

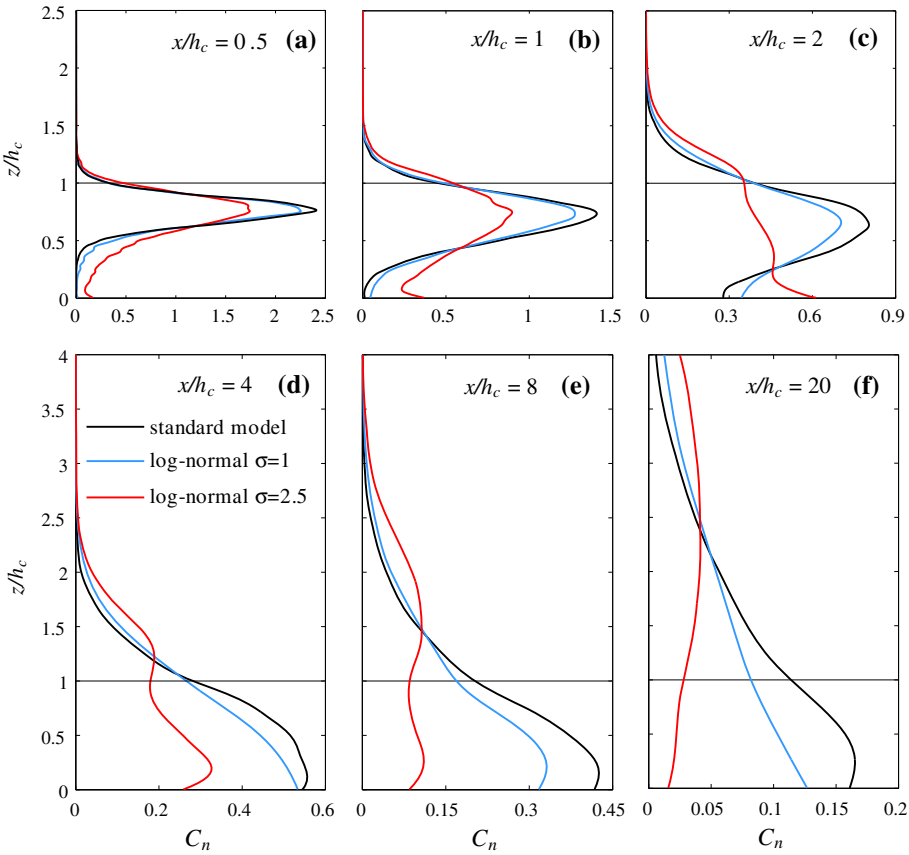

Fig. 7 Modelled profiles of normalized mean concentration C_{n} at different distances from the source location for a canopy flow ($C_\chi = 1.6$)

canopy is governed mostly by the scales of the canopy height, while the particles that are reflected from the top of the boundary layer are "trapped" above the canopy and rarely affect the concentration within the canopy.

Vertical profiles of concentration (Fig. 7) show distinctly higher dispersion close to the source in the upwind direction, which is amplified by the addition of the log-normal model. For $\sigma = 2.5$, the canopy effect is much more evident, showing two peaks in concentration, one below the canopy and one above. The high concentration above the canopy is created by the ejection of particles, and at $x = 20h_{\mathrm{c}}$ (Fig. 7f) the concentration distribution is reversed for high values of σ, where the concentration above the canopy is higher than the concentration within the canopy.

For canopy flows, the importance of the near-field region is quite significant despite its restricted extent. From Fig. 6, the near-field region is shown to extend to only about $2h_{\mathrm{c}}$, and the effect of intermittency in this region cannot be ignored. The enhanced ejection phase may lead to more frequent particle escapes from the canopy volume and promote longer-dispersal distances from the source. Concentration and flux footprints are likely to be influenced even more by increases in high dissipation events due to their high sensitivity to the dispersion at the source location.

6 Conclusions

In this work, the conventional Lagrangian trajectory approach is expanded to include a stochastic model for the instantaneous dissipation rate that is based on a log-normal distribution law. This novel approach is employed to conduct trajectory simulations in highly inhomogeneous atmospheric turbulent flows. Using multi-level field measurements from a pine forest, it is demonstrated that instantaneous dissipation rates in canopy flows are reasonably log-normally distributed, and that the relative variability in the mean dissipation rate far exceeds those reported in DNS studies at moderate Reynolds number. These results (empirically) suggest that incorporating the variability in the TKE dissipation rate is warranted for such an atmospheric flow system.

The proposed model demonstrates that the addition of dissipation rate variability amplifies two types of motion governing the spatial evolution of the mean concentration with increasing distance from an elevated source. The first is connected to strong sweeping motion that enhances the decay rate of the mean concentration with increased downwind distance, and the second is linked to strong intermittent ejections of particles from the canopy immediately adjacent to the source. Shortly after their release, these particles escape the low-velocity region within the canopy volume to a high-velocity region in the free air above the canopy via a strong ejection motion. This ejective phenomenon increases the probability of single particles to reach far regions, creating a heavy tail in the mean concentration far from the scalar source. These types of motion for now should be treated as model-based conjectures that cannot be directly predicted using standard LS approaches. A direct verification of their importance may be achieved using scalar release experiments. However, such experiments may be complicated by the fast decay of tracer concentration near the source.

With regards to applications, especially those pertinent to inverse modeling, the extended model can be readily used to compute the elements of a dispersion matrix (i.e. how a unit source at position i affects the concentration at location j) employed in common inverse schemes such as the localized near-field theory. Also, the extended model can be coupled to inertial particle trajectories along similar lines as is done for conventional LS models. Such an extension allows variability in ϵ^* to be included in seed and pollen dispersion, the subject of future work.

Acknowledgments This work was supported by Research Grant Award No. IS-4374-11C from BARD, the United States—Israel Binational Agricultural Research and Development Fund.

Appendix 1: Verification of the Well-Mixed Condition for the Log-Normal Model

All LS models used for turbulent dispersion must satisfy the so-called well-mixed condition (Thomson 1987). According to the well-mixed condition, particles of a tracer initially well-mixed in a turbulent flow must remain well-mixed at all times. The formulation of the drift and dispersion in the standard model by Thomson (1987) satisfies the well-mixed condition. In the log-normal model the well-mixed condition should be preserved by the construction of the model. However, this model is new and therefore the log-normal model must be first tested before being applied especially for the inhomogeneous flows considered here.

Here two checks are conducted—a theoretical one to assess whether the formulation of the log-normal model satisfies the well-mixed condition, and a numerical one where the log-normal model is tested for a case of strong inhomogeneous flow.

The Well-Mixed Condition: Formulation Analysis of the Log-Normal Model

By construction the model considered in the manuscript satisfies the well-mixed condition and has independent one-point one-time Eulerian PDFs of velocity and dissipation, i.e. the joint PDF of velocity and logarithm of the normalized dissipation $f_{\mathrm{E}}^{u\chi}$ can be simply written as $f_{\mathrm{E}}^{u\chi} = f_{\mathrm{E}}^{u} f_{\mathrm{E}}^{\chi}$.

These properties can be shown starting from a general model of the form,

$$\mathrm{d}u_i = a_i(\mathbf{x}, \mathbf{u}, \epsilon)\mathrm{d}t + b_{ij}(\epsilon)\mathrm{d}W_j, \tag{10}$$

$$\mathrm{d}x_i = u_i \mathrm{d}t, \tag{11}$$

$$\mathrm{d}\chi = M(\chi)\mathrm{d}t + D\mathrm{d}W, \tag{12}$$

where, $M(\chi) = -(\chi - \langle\chi\rangle)/T_\chi$, $D = \sqrt{2\sigma^2/T_\chi}$, and $\epsilon = \langle\epsilon\rangle \exp(\chi)$. For simplicity and convenience ϵ is used here for the random dissipation (instead of ϵ^*), and $\langle\epsilon\rangle$ stands for the averaged dissipation. Moreover, no special notation is used for the particle random variable appearing in the stochastic differential equation (SDE), although it must be understood that here the SDE refers to the Lagrangian particle quantity.

The previous system of SDE satisfies a Fokker–Planck equation for the Lagrangian joint PDF $f_{\mathrm{L}}^{u\chi}$ and, by the relation between Lagrangian and Eulerian PDFs (e.g. Novikov 1969, 1986; Pope and Chen 1990; Pope 2000; Thomson 1987), the one-point one-time Eulerian PDF $f_{\mathrm{E}}^{u\chi}$ satisfies as well a Fokker–Plank equation of the form,

$$\frac{\partial f_{\mathrm{E}}^{u\chi}}{\partial t} + \frac{\partial u_i f_{\mathrm{E}}^{u\chi}}{\partial x_i} + \frac{\partial a_i f_{\mathrm{E}}^{u\chi}}{\partial u_i} - \frac{1}{2} b_{ik} b_{kj} \frac{\partial^2 f_{\mathrm{E}}^{u\chi}}{\partial u_i \partial u_j} + \frac{\partial M f_{\mathrm{E}}^{u\chi}}{\partial \chi}. - \frac{1}{2} \frac{\partial^2 D^2 f_{\mathrm{E}}^{u\chi}}{\partial \chi \partial \chi} = 0 \tag{13}$$

This equation is general and does not assume that the two PDFs are independent. Assuming independency $f_{\mathrm{E}}^{u\chi} = f_{\mathrm{E}}^{u} f_{\mathrm{E}}^{\chi}$ and integrating over the whole space of the variable χ (under some regularity conditions, see e.g. Pope (2000), p. 466 and Thomson (1987), p.534, it is possible to obtain an equation for the marginal PDF f_{E}^{u},

$$\frac{\partial f_{\mathrm{E}}^{u}}{\partial t} + \frac{\partial u_i f_{\mathrm{E}}^{u}}{\partial x_i} + \frac{\partial \langle a_i\rangle^{\chi} f_{\mathrm{E}}^{u}}{\partial u_i}, - \frac{1}{2} \left\langle b_{ik} b_{kj} \right\rangle^{\chi} \frac{\partial^2 f_{\mathrm{E}}^{u}}{\partial u_i \partial u_j} = 0 \tag{14}$$

where the notation $\langle\,\rangle^{\chi}$ $\left(\equiv \int_{-\infty}^{\infty} f_{\mathrm{E}}^{\chi} \mathrm{d}\chi\right)$ indicates that the average is taken only over the space of χ. With the choice of $b_{ij}(\epsilon) = \sqrt{C_0\epsilon}\delta_{ij}$ used here, and by noting that $\langle\epsilon\rangle^{\chi} = \langle\langle\epsilon\rangle \exp(\chi)\rangle^{\chi} = \langle\epsilon\rangle \langle\exp(\chi)\rangle^{\chi} = \langle\epsilon\rangle$, since χ is normalized so that $\langle\exp(\chi)\rangle^{\chi}$ is unity (Pope and Chen 1990), we have,

$$\frac{\partial f_{\mathrm{E}}^{u}}{\partial t} + \frac{\partial u_i f_{\mathrm{E}}^{u}}{\partial x_i} + \frac{\partial \langle a_i\rangle^{\chi} f_{\mathrm{E}}^{u}}{\partial u_i} - \frac{1}{2} C_0 \langle\epsilon\rangle \frac{\partial^2 f_{\mathrm{E}}^{u}}{\partial u_i \partial u_i} = 0. \tag{15}$$

If we assume a pre-defined form of f_{E}^{u} we obtain from the previous equation that

$$\langle a_i\rangle^{\chi} = \frac{1}{f_{\mathrm{E}}^{u}} \left(\frac{1}{2} C_0 \langle\epsilon\rangle \frac{\partial f_{\mathrm{E}}^{u}}{\partial u_i} + \Phi_i(u_i) \right), \tag{16}$$

where Φ_i is as defined by Thomson (1987) Eq. 9b (for more details see Rodean 1996, Chap. 8). Satisfying this condition ensures that the model has independent PDFs ($f_{\mathrm{E}}^{u\chi} = f_{\mathrm{E}}^{u} f_{\mathrm{E}}^{\chi}$) and that the Eulerian velocity PDF is a solution to Eq. 15. However, this is a necessary but not sufficient condition for the well-mixed condition since it does not define the drift coefficient a_i in Eq. 10 but only its averaged value. Indeed, looking at Eqs. 10 and 11 seperately from

Eq. 12 we obtain another Fokker-Plank transport equation that the Eulerian velocity PDF f_{E}^{u} must satisfy (given $b_{ij}(\epsilon) = \sqrt{C_0\epsilon}\delta_{ij}$),

$$\frac{\partial f_{\mathrm{E}}^{u}}{\partial t} + \frac{\partial u_i f_{\mathrm{E}}^{u}}{\partial x_i} + \frac{\partial a_i f_{\mathrm{E}}^{u}}{\partial u_i} - \frac{1}{2}C_0\epsilon\frac{\partial^2 f_{\mathrm{E}}^{u}}{\partial u_i \partial u_i} = 0. \tag{17}$$

Satisfying the well-mixed condition (i.e. the fact that a given f_{E}^{u} is a solution of Eq. 17) brings to the definition of the drift coefficient used here,

$$a_i = \frac{1}{f_{\mathrm{E}}^{u}}\left(\frac{1}{2}C_0\epsilon\frac{\partial f_{\mathrm{E}}^{u}}{\partial u_i} + \Phi_i(u_i)\right), \tag{18}$$

where Φ_i is again as defined by Thomson (1987). Comparing the definition in Eqs. 18 and 16, we see that Eq. 18 respects Eq. 16 since upon ensemble averaging of Eq. 18 over the space of χ, Eq. 16 is retrieved. Therefore, Eq. 18 is more restrictive, and its definition of the drift coefficient is necessary and sufficient for the well-mixed condition to be satisfied. Also, since Eq. 18 contains Eq. 16 it also turns out that f_{E}^{u} and f_{E}^{χ} are independent.

The Well-Mixed Test

For the well-mixed test, a highly inhomogeneous canopy flow dataset was selected from an open-channel experiment, where laser Doppler anemometry measurements were available for all flow statistics (Poggi et al. 2006). For this type of flow, all the terms of the drift coefficients a_u and a_w are included (Eqs. 3, 4), so the most general form of the model can be examined. In all simulations, the particles that reach the ground or the water level, which extends to $5h_{\mathrm{c}}$, are reflected in the vertical direction and the sign of their velocity fluctuations is also reversed. Since the canopy domain and the free flow domain above the canopy are of the same order of magnitude and have a distinct differences in the flow statistics, the test is presenting an extreme flow environment to the LS model in terms of flow inhomogeneity.

The flow conditions are described in Poggi et al. (2006) and the flow statistics are shown in their Fig. 2. In each test 5×10^6 particles were released uniformly across all z at $x = 0$. The trajectories were computed using the LS equations (Eqs. 1–7) for some 150 s—sufficiently enough to test whether they truly stay well-mixed over time. The log-normal model parameters were set to $\sigma = 1$ or 2.5, and $C_\chi = 0.5$, 1.6 or 3. For details about the choice of σ and C_χ, see Sects. 3 and 4 respectively. At the end of the simulation, the domain was divided into 50 vertical layers, and the number of particles in each layer was computed and then divided by the expected well-mixed value. a perfectly well-mixed distribution of the horizontally integrated concentration should be unity in each layer.

The test results clearly show that the well-mixed condition is satisfied for all the simulations. Figure 8 shows the normalized concentration at the end of the well-mixed test simulations for the log-normal model with $\sigma = 1$ and 2.5 for $C_\chi = 1.6$, compared with the results for the standard model. The particle distribution is equal to the expected well-mixed concentration at all heights with an error of less than 2 %. All the other tests (for $C_\chi = 0.5$ and 3) gave similarly good results and are not shown here. These results verify that the log-normal model satisfies the well-mixed condition, and may be used to perform correct dispersion simulations in inhomogeneous atmospheric flows.

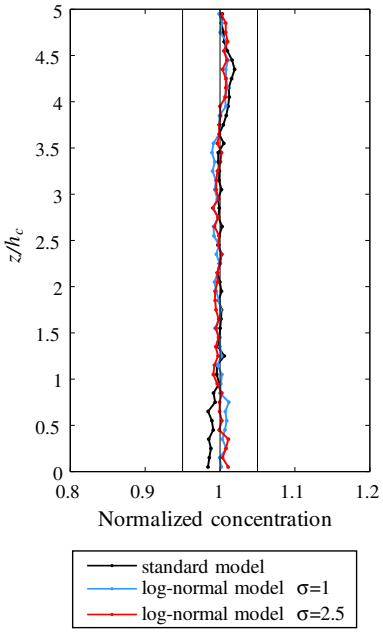

Fig. 8 The verification of the well-mixed condition: final particle distribution normalized by the expected well-mixed value. The *vertical lines* stand for a perfectly well-mixed distribution (at 1), and an error of ±5 %

Appendix 2: Atmospheric Boundary-Layer Flow Statistics (MOST)

The profiles of the Eulerian flow statistics needed in the ABL case study are presented here. These include the mean velocity, its SD, the Reynolds stress, and the mean dissipation rate (or integral time scale). Using Monin–Obukhov similarity theory, the following profiles were employed for neutral, stable and unstable conditions (Kaimal and Finnigan 1994).

The mean wind speed $\overline{u}(z)$ is calculated as

$$\overline{u}(z) = \frac{k}{u_*}\left(\ln\left(\frac{z}{z_0}\right) - \psi\right), \tag{19}$$

where $k = 0.4$ is the von Karman constant, u_* is the friction velocity, and z_0 is the aerodynamic roughness length. The values of the last two were set to $u_* = 0.4\,\mathrm{m\,s^{-1}}$ and $z_0 = 1.7$ mm in all ABL simulations.

ψ is the stability correction function, which is expressed by,

$$\begin{aligned} &\psi(z) = -5z/L, && \text{for } z/L \geq 0 \\ &\psi(z) = 2\ln\left(\tfrac{1+\phi}{2}\right) + \ln\left(\tfrac{1+\phi^2}{2}\right) - 2\tan^{-1}(\phi) + \tfrac{\pi}{2} && \text{for } z/L < 0, \end{aligned} \tag{20}$$

where the Obukhov length L was chosen to be 200 for stable conditions, -10 for unstable conditions, and ϕ is given by: $\phi(z) = (1 - 16z/L)^{1/4}$. For neutral conditions $L \to \infty$, and therefore $\psi = 0$.

The velocity SD profiles are expressed as,

$$\begin{aligned} &\sigma_u = 2.5u_*, && \sigma_w = 1.25u_*, && \text{for } z/L \geq 0 \\ &\sigma_u = 2.5u_*\left(1 - 3\tfrac{z}{L}\right)^{1/3}, && \sigma_w = 1.25u_*\left(1 - 3\tfrac{z}{L}\right)^{1/3} && \text{for } z/L < 0. \end{aligned} \tag{21}$$

The Reynolds stress is constant for all stability conditions: $\overline{u'w'} = -u_*^2$.

Finally, the Lagrangian time scale is estimated using the diffusion coefficient according to K theory as $T_{\mathrm{L}} = K/\sigma_w^2$ (Rodean 1996), and the mean dissipation rate is calculated from the consistency with the Kolmogorov's similarity theory for locally isotropic turbulence as $\epsilon = 2\sigma_w^2/C_0 T_{\mathrm{L}}$. C_0 is a phenomenological constant, taken to be 3.125, based on matching of the Lagrangian time scale to similarity theory (Li and Taylor 2005), and the diffusion coefficient is estimated by $K(z) = kzu_*/\phi_h$, with ϕ_h given by (Hsieh et al. 2000),

$$\begin{aligned} \phi_h(z) &= 1 + 5\tfrac{z}{L}, && \text{for } z/L \geq 0 \\ \phi_h(z) &= 0.032\left(0.037 - \tfrac{z}{L}\right)^{-1/3}. && \text{for } z/L < 0 \end{aligned} \tag{22}$$

For stable conditions ($z/L > 0$) all the correction functions are stretched to the top of the ABL (taken as 300 m for this case). For the unstable conditions ($z/L < 0$), the corrections are used only for the surface layer, which is estimated as 20 % of the entire height of the ABL (200 m of the 1 km height of the ABL). Above this height, in the mixed layer, all the statistics are taken as constants for the unstable case.

References

Anand M, Pope S, Mongia H (1993) Pdf calculations for swirling flows. In: Proceedings of 31st aerospace sciences meeting and exhibition, Reno, NV. AIAA Paper 93–0106

Antonia R (1973) Some small scale properties of boundary layer turbulence. Phys Fluids 16:1198–1206

Baldocchi D (1997) Flux footprints within and over forest canopies. Boundary-Layer Meteorol 85(2):273–292

Cassiani M, Franzese P, Giostra U (2005a) A PDF micromixing model of dispersion for atmospheric flow. Part I: development of the model, application to homogeneous turbulence and to neutral boundary layer. Atmos Environ 39(8):1457–1469

Cassiani M, Radicchi A, Giostra U (2005b) Probability density function modelling of concentration fluctuation in and above a canopy layer. Agric For Meteorol 133:153–165

Chen W (1971) Lognormality of small-scale structure of turbulence. Phys Fluids 14:1639–1642

Finnigan J (2000) Turbulence in plant canopies. Annu Rev Fluid Mech 32:519–571

Flesch T, Wilson J (1992) A two-dimensional trajectory-simulation model for non-Gaussian, inhomogeneous turbulence within plant canopies. Boundary-Layer Meteorol 61:349–374

Flesch TK, Wilson JD, Yee E (1995) Backward-time Lagrangian stochastic dispersion models and their application to estimate gaseous emissions. J Appl Meteorol 34(6):1320–1332

Freytag C (1978) Statistical properties of energy dissipation. Boundary-Layer Meteorol 14(2):183–198

Frisch U (1996) Turbulence: the legacy of A. N. Kolmogorov. Cambridge University Press, Cambridge, 296 pp

Hsieh C, Katu G, Chi T (2000) An approximate analytical model for footprint estimation of scalar fluxes in thermally stratified atmospheric flows. Adv Water Resour 23(7):765–772

Hsieh CI, Katul G (2009) The Lagrangian stochastic model for estimating footprint and water vapor fluxes over inhomogeneous surfaces. Int J Bioclimatol Biometeorol 53(1):87–100

Juang J, Katul G, Siqueira M, Stoy P, Palmroth S, McCarthy HR, Kim H, Oren R (2006) Modeling nighttime ecosystem respiration from measured CO_2 concentration and air temperature profiles using inverse methods. J Geophys Res 111:D08S05

Juang J, Katul G, Siqueira M, McCarthy H (2008) Investigating a hierarchy of eulerian closure models for scalar transfer inside forested canopies. Boundary-Layer Meteorol 128:1–32

Kaimal J, Finnigan J (1994) Atmospheric boundary layer flows: their structure and measurement. Oxford University Press, New York, 289 pp

Katul G, Albertson J (1998) An investigation of higher-order closure models for a forested canopy. Boundary-Layer Meteorol 89(1):47–74

Kljun N, Rotach N, Schmid H (2002) A three-dimensional backward Lagrangian footprint model for a wide range of boundary-layer stratifications. Boundary-Layer Meteorol 103:205–226

Kolmogorov A (1962) A refinement of previous hypotheses concerning the local structure of turbulence in a viscous incompressible fluid at high Reynolds number. J Fluid Mech 13:82–85

Kurbanmuradov O, Sabelfeld K (2000) Lagrangian stochastic models for turbulent dispersion in the atmospheric boundary layer. Boundary-Layer Meteorol 97(2):191–218

Leuning R, Denmead O, Miyata A, Kim J (2000) Source/sink distributions of heat, water vapor, carbon dioxide, and methane in a rice canopy estimated using lagrangian dispersion analysis. Agric For Meteorol 103:233–249
Li P, Taylor P (2005) Three-dimensional Lagrangian simulation of suspended particles in the neutrally stratified atmospheric surface layer. Boundary-Layer Meteorol 116(2):301–311
Minier J, Pozorski J (1999) Wall-boundary conditions in probability density function methods and application to a turbulent channel flow. Phys Fluids 11:2632–2644
Monin A, Yanglom A (1975) Statistical fluid mechanics: mechanics of turbulence, vol 2. MIT Press, Cambridge, 874 pp
Nathan R, Katul G, Horn H, Thomas S, Oren R, Avissar R, Pacala S, Levin S (2002) Mechanisms of long-distance dispersal of seeds by wind. Nature 418(6896):409–413
Nemitz E, Sutton M, Gut A, San-José R, Husted S, Schjoerring J (2000) Sources and sinks of ammonia within an oilseed rape canopy. Agric For Meteorol 105:385–404
Novikov E (1969) Relation between the Lagrangian and Eulerian descriptions of turbulence. J Appl Math Mech 33(5):862–864
Novikov E (1986) The Lagrangian–Eulerian probability relations and the random force method for nonhomogeneous turbulence. Phys Fluids 29(12):3907–3909
Obukhov A (1962) Some specific features of atmospheric turbulence. J Geophys Res 67:3011–3014
Poggi D, Katul G, Albertson J (2004) Momentum transfer and turbulent kinetic energy budgets within a dense model canopy. Boundary-Layer Meteorol 111:589–614
Poggi D, Katul G, Albertson J (2006) Scalar dispersion within a model canopy: measurements and three-dimensional Lagrangian models. Adv Water Resourc 29(2):326–335
Pope S (1991) Application of the velocity–dissipation probability density function model to inhomogeneous turbulent flows. Phys Fluids A 3:1947–1957
Pope S (2000) Turbulent flows. Cambridge University Press, Cambridge, 771 pp
Pope S, Chen Y (1990) The velocity–dissipation probability density function model for turbulent flows. Phys Fluids A 2:1437–1449
Porta AL, Voth GA, Crawford AM, Alexander J, Bodenschatz E (2001) Fluid particle accelerations in fully developed turbulence. Boundary-Layer Meteorol 409:1017–1019
Rannik Ü, Aubinet M, Kurbanmuradov O, Sabelfeld K, Markkanen T, Vesala T (2000) Footprint analysis for measurements over a heterogeneous forest. Boundary-Layer Meteorol 97(1):137–166
Raupach M (1989) Applying Lagrangian fluid-mechanics to infer scalar source distributions from concentration profiles in plant canopies. Agric For Meteorol 47:85–108
Raupach M, Thom A (1981) Turbulence in and above plant canopies. Annu Rev Fluid Mech 13:97–129
Rodean H (1996) Stochastic Lagrangian models of turbulent diffusion. Meteorological monographs, vol 26, no. 48. American Meteorological Society, Boston, 84 pp
Simon E, Lehmann B, Ammann C, Ganzeveld L, Rummel U, Meixner F, Nobre A, Araujo A, Kesselmeier J (2005) Lagrangian dispersion of ^{222}Rn, H_2O and CO_2 within Amazonian rain forest. Agric For Meteorol 132:286–304
Siqueira M, Lai C, Katul G (2000) Estimating scalar sources, sinks, and fluxes in a forest canopy using Lagrangian, Eulerian, and hybrid inverse models. J Geophys Res 105:29475–29488
Siqueira M, Katul G, Lai C (2002) Quantifying net ecosystem exchange by multilevel ecophysiological and turbulent transport models. Adv Water Resour 25:1357–1366
Siqueira M, Leuning R, Kolle O, Kelliher F, Katul G (2003) Modeling sources and sinks of CO_2, H_2O and heat within a Siberian pine forest using three inverse methods. Q J R Meteorol Soc 129:1373–1393
Siqueira M, Katul G, Tanny J (2012) The effect of the screen on the mass, momentum, and energy exchange rates of a uniform crop situated in an extensive screenhouse. Boundary-Layer Meteorol 142(3):339–363
Taylor G (1921) Diffusion by continuous movements. Proc Lond Math Soc 20:196–211
Thomson D (1987) Criteria for the selection of stochastic models of particle trajectories in turbulent flows. J Fluid Mech 180:529–556
Tiwary A, Fuentes J, Barr J, Wang D, Colls J (2007) Inferring the source strength of isoprene from ambient concentrations. Environ Modell Softw 22:1281–1293
Vesala T, Kljun N, Rannik U, Rinne J, Sogachev A, Markkanen T, Sabelfeld K, Foken T, Leclerc M (2008) Flux and concentration footprint modelling: state of the art. Environ Pollut 152(3):653–666
Wilson J (1988) A second order closure model for flow through vegetation. Boundary-Layer Meteorol 42: 371–392
Wilson JD, Sawford BL (1996) Review of Lagrangian stochastic models for trajectories in the turbulent atmosphere. Boundary-Layer Meteorol 78:191–210
Yeung P, Pope S (1989) Lagrangian statistics from direct numerical simulations of isotropic turbulence. J Fluid Mech 207:581–586